Auxiliary boson approach for electronic states in the two-dimensional Hubbard model

T. Saikawa, A. Ferraz, and P. E. de Brito*
Centro Internacional de Física da Matéria Condensada-ICCMP, Universidade de Brasília, CEP 70919-970 Brasília-DF, Brazil

H. Kaga
Department of Physics, Niigata University, Niigata 950-21, Japan
(Received 3 February 1997)

Electronic states in the two-dimensional Hubbard model are studied in the doped paramagnetic states by use of the auxiliary boson approach. Four auxiliary bosons are introduced by means of the Hubbard-Stratonovich transformation within the functional integral treatment. These bosons correspond to one charge and three spin fluctuations. An effective model is formulated. Going beyond the boson fluctuations around the saddle point, the single-electron Green's function including one-loop self-energy effects of fermion-boson interaction is derived. The behavior of the fermion self-energy, spectral functions, and density of states are investigated for several values of the Coulomb interaction U within the limit imposed by the Stoner criterion and also for small and moderate doping concentrations δ. For small doping ($\delta=0.2$), as U approaches a value determined by the Stoner criterion, the spin-boson spectrum has a striking low-energy enhancement around $\mathbf{q}\sim 2\mathbf{k}_F$. This enhancement of the spin fluctuation causes a non-Fermi-liquid-like low-energy ω linear dependence in the imaginary part of the self-energy. Due to the self-energy effects, band splittings and a band narrowing are produced in the spectral functions. As a consequence of this, the density of states has pseudogap structures around the quasiparticle band with a narrow bandwidth on the Fermi energy. These features seem to be precursors of the metal-insulator (Mott-Hubbard) transition and they might be related to the spin-gap phenomena observed in high-T_c materials. Our results for the density of states, the spectral function, and the band dispersions show qualitative agreement with the data of finite-size cluster simulations.
[S0163-1829(97)05031-5]

I. INTRODUCTION

High-T_c materials have a number of unusual physical properties[1] that are not easy to understand within the framework of the Fermi-liquid theory. There are many open questions concerning these materials. For example, the origin of the pseudogap (spin-gap) in the spin excitation spectrum,[2,3] the pseudogap in the normal-state excitation spectrum,[4,5] and finally the possibility of the spin-charge separation[6–8] in the two-dimensional strongly correlated electron systems. These phenomena must be closely related to the anomalous metallic states near the metal-insulator transition due to the strong Coulomb interaction between two electrons on each Cu site. To understand the anomalous metallic states and to solve these questions, we must get a better physical picture of the electronic states of these materials. It is a basic problem to understand the essential features of the strongly correlated electron systems.

After the discovery of high-T_c materials, the single-band Hubbard model, the three-band CuO_2 model, and the t-J model have been studied intensively to investigate the origin of the above-mentioned phenomena and also to calculate the high superconducting transition temperature. Among these, the single-band Hubbard model is the most fundamental model to describe the metal-insulator transition due to the strong electron-electron interaction on the lattice electron system and also to investigate the nature of the anomalous metallic state near the metal-insulator transition. The Hubbard model seems to be oversimplified to describe the electronic states of the high-T_c materials. However, this model contains the correct nature of the strongly correlated system and it provides very useful information for more realistic models, which are more favorable to study the properties of the high-T_c cuprates.

Though the Hamiltonian is of a simple form, because of the large Coulomb interaction, it is difficult to pursue detailed investigation of the electronic states near the metal-insulator transition. As in the early investigations of the Hubbard model, two methods are known well. One is the Hubbard approximation,[9] based on the equation of motion method, and the other is the Gutzwiller variational function method.[10] At first sight the two approaches seem to give different descriptions of the metal-insulator transition. In the former approach the density of states (DOS) shows the band gap (Mott-Hubbard gap) at the critical value of the Coulomb interaction. The latter explains the metal-insulator transition by the band narrowing effects, i.e., by the localization of the quasiparticle band. These two different explanations of the metal-insulator transition have been shown to be essential features of the metal-insulator transition described by the Hubbard model.

This has been shown theoretically using the slave-boson method[11] and was also demonstrated clearly by the numerical simulation approaches[12–19] and the $d=\infty$ method.[20] By the recent progress in the capability of computers many interesting results have been obtained in the numerical simulations of the finite-size cluster systems.[12–19] Although a restriction on the size of the system and temperature exists, these methods seem to simulate to some extent, in a correct manner, the essential properties of the single-particle spec-

trum in the Hubbard model. The $d=\infty$ method is also one of the most effective methods to study strongly correlated systems.[20] This method is particularly useful in revealing the nature of the density of states in the infinite-dimensional Hubbard model. At half filling and for a critical Coulomb interaction U_C the physical system becomes insulating. From these approaches one realizes that there are some common properties in the electronic states of the Hubbard model: (i) for $0 \ll U < U_C$ the DOS has three characteristic band structures; one lower and one upper Hubbard band in the high-energy region and one narrow quasiparticle band on the Fermi level; (ii) for hole (electron) dopings, quasiparticle band structure appears at the top (bottom) of the lower (upper) Hubbard band. Recently, these features have been obtained also by the composite operator expansion methods, which take into account the two-site correlation effect.[21]

In this paper we investigate the evolution of the electronic states of the two-dimensional Hubbard model with the change of the Coulomb interaction U and the doping concentration δ. Our main purpose in this study is to investigate the detailed behavior of the single-particle spectra taking into account the effects of the charge and spin fluctuations. We introduce four auxiliary bosons to consider both charge and spin fluctuations in the interaction term of the Hubbard Hamiltonian. One effective model is constructed in the functional integral formulation. The boson fluctuations around the saddle point are taken into account and the Dyson equations for both the boson propagators and the fermion Green's function are derived by the explicit calculation of the self-energies up to one-loop order. Within the critical value of the Coulomb interaction controlled by the Stoner instability criterion,[22] we calculate the real and the imaginary parts of the self-energies, the spectral functions, and the density of states. For large U, the energy dependence of the imaginary part of the self-energy at the wave vector near the Fermi surface becomes linear in energy around the Fermi energy. The effective band dispersion deduced from the data of the spectral function demonstrates the onset of gap formation in the high-energy region. This effect reflects itself in the density of states since there appears a pseudogap structure around the narrow quasiparticle band for large U. These features in the single-particle spectrum coincide qualitatively with results obtained in the numerical simulations, the $d=\infty$ method, and also by the composite operator method. It will be shown that the strong enhancement of the low-energy spin excitation near $\mathbf{q} \sim 2\mathbf{k}_F$ for the low doping concentration causes a non-Fermi-liquid-like behavior in the electronic states in the Hubbard model.

II. AUXILIARY BOSON APPROACH

We consider the interacting electron system in a two-dimensional square lattice with unit lattice constant at zero temperature. The system is described by the following Hubbard Hamiltonian:

$$H = H_0 + H', \tag{2.1}$$

$$H_0 = -t \sum_{\langle i,j \rangle,\sigma} c_{i\sigma}^{\dagger} c_{j\sigma} - \mu \sum_{i,\sigma} n_{i\sigma}, \tag{2.2}$$

$$H' = U \sum_i n_{i\uparrow} n_{i\downarrow}, \tag{2.3}$$

where $c_{i\sigma}^{\dagger}$ ($c_{i\sigma}$) represents the electron creation (annihilation) operator on an orbital of the ith lattice site with spin σ, t is the nearest-neighbor hopping energy, and μ is the chemical potential. The index i of the summation of the first term in H_0 runs all over the lattice sites and j runs over nearest-neighbor sites of each ith site. In the interaction Hamiltonian H', U is the coupling constant of the Coulomb interaction between two electrons with opposite spin directions on a same lattice site. $n_{i\sigma} = c_{i\sigma}^{\dagger} c_{i\sigma}$ is the number operator of electrons on the ith site with spin σ. Using the charge-density operator n_i defined by

$$n_i = \sum_{\sigma} n_{i\sigma} \tag{2.4}$$

and the spin-density vector operator $\mathbf{s}_i = (s_i^{(1)}, s_i^{(2)}, s_i^{(3)})$ defined by

$$\mathbf{s}_i = \frac{1}{2} \sum_{\sigma,\sigma'} c_{i\sigma}^{\dagger} \boldsymbol{\tau}_{\sigma\sigma'} c_{i\sigma'} \tag{2.5}$$

where $\boldsymbol{\tau}$ is the Pauli matrix with components

$$\boldsymbol{\tau}^{(1)} = \begin{pmatrix} 0 & 1 \\ 1 & 0 \end{pmatrix}, \quad \boldsymbol{\tau}^{(2)} = \begin{pmatrix} 0 & -i \\ i & 0 \end{pmatrix}, \quad \boldsymbol{\tau}^{(3)} = \begin{pmatrix} 1 & 0 \\ 0 & -1 \end{pmatrix}, \tag{2.6}$$

we rewrite the interaction term as

$$H' = \frac{U}{2} \sum_i \left\{ \left(\frac{n_i}{2} \right)^2 - \mathbf{s}_i^2 \right\}. \tag{2.7}$$

Furthermore, by introducing the 2×2 unit matrix $\boldsymbol{\tau}^{(0)} = \mathbf{1}$ the interaction Hamiltonian can be written in a simpler form as

$$H' = \frac{U}{2} \sum_i \sum_{a,b=0}^{3} s_i^{(a)} \eta_{ab} s_i^{(b)}, \tag{2.8}$$

where

$$s_i^{(a)} = \frac{1}{2} \sum_{\sigma,\sigma'} c_{i\sigma}^{\dagger} \tau_{\sigma\sigma'}^{(a)} c_{i\sigma'}, \tag{2.9}$$

and η_{ab} is an element of the matrix $\boldsymbol{\eta}$ defined by

$$\boldsymbol{\eta} = \begin{bmatrix} 1 & 0 & 0 & 0 \\ 0 & -1 & 0 & 0 \\ 0 & 0 & -1 & 0 \\ 0 & 0 & 0 & -1 \end{bmatrix}. \tag{2.10}$$

In the functional integral formulation[23,24] the partition function Z of the system is given by

$$Z = \int D\Psi^{\dagger} D\Psi \exp\left(i \int dt \sum_{\mathbf{r}} \mathcal{L} \right) \tag{2.11}$$

with the Lagrangian density $\mathcal{L}$ defined by

$$\mathcal{L}=\sum_{\sigma}\Psi^{\dagger}_{\sigma}(\mathbf{r},t)(i\partial_t+\mu)\Psi_{\sigma}(\mathbf{r},t)+t\sum_{j=x,y}\sum_{\sigma}\Psi^{\dagger}_{\sigma}(\mathbf{r},t)\times\Psi_{\sigma}(\mathbf{r}\pm\mathbf{e}_j,t)-\frac{U}{2}\sum_{a,b=0}^{3}s^{(a)}(\mathbf{r},t)\,\eta_{ab}s^{(b)}(\mathbf{r},t), \tag{2.12}$$

where $\Psi^{\dagger},\Psi$ are Grassmann fields, $\mathbf{e}_j$ is the unit lattice vector for j direction, and

$$s^{(a)}(\mathbf{r},t)=\frac{1}{2}\sum_{\sigma,\sigma'}\Psi^{\dagger}_{\sigma}(\mathbf{r},t)\,\tau^{(a)}_{\sigma\sigma'}\Psi_{\sigma'}(\mathbf{r},t). \tag{2.13}$$

We introduce four auxiliary bosonic operators $\phi^{(a)}(\mathbf{r},t)$ for the charge-density $(a=0)$ and the spin-density $(a=1,2,3)$ operators through the Hubbard-Stratonovich relation

$$\int d\phi^{(a)}\exp i\left[\frac{1}{2}\phi^{(a)}\eta_{ab}\phi^{(b)}+\sqrt{U}\phi^{(a)}\eta_{ab}s^{(b)}\right]=\text{const}\ \exp\left[-i\frac{U}{2}s^{(a)}\eta_{ab}s^{(b)}\right]. \tag{2.14}$$

Performing a Hubbard-Stratonovich transformation we obtain

$$Z=\int D\Psi^{\dagger}D\Psi D\phi\exp\left(i\int dt\sum_{\mathbf{r}}\mathcal{L}'\right) \tag{2.15}$$

with the Lagrangian density

$$\mathcal{L}'=\sum_{\sigma}\Psi^{\dagger}_{\sigma}(\mathbf{r},t)(i\partial_t+\mu)\Psi_{\sigma}(\mathbf{r},t)+t\sum_{j=x,y}\sum_{\sigma}\Psi^{\dagger}_{\sigma}(\mathbf{r},t)\Psi_{\sigma}(\mathbf{r}\pm\mathbf{e}_j,t)+\frac{\sqrt{U}}{2}\sum_{\sigma,\sigma'}\sum_{a,b}\eta_{ab}\phi^{(a)}(\mathbf{r},t)\Psi^{\dagger}_{\sigma}(\mathbf{r},t)\,\tau^{(b)}_{\sigma\sigma'}\Psi_{\sigma'}(\mathbf{r},t)+\frac{1}{2}\sum_{a,b}\phi^{(a)}(\mathbf{r},t)\,\eta_{ab}\phi^{(b)}(\mathbf{r},t). \tag{2.16}$$

Thus, we consider the system of fermions and bosons with a Yukawa-type interaction between fermions and bosons instead of the quartic order term of fermion fields.[24]

By integrating out the Grassmann fields we immediately obtain effective action for the boson system as follows:

$$Z=\int D\phi\exp[iS_{\text{eff}}(\phi)], \tag{2.17}$$

$$S_{\text{eff}}(\phi)=\int dt\sum_{\mathbf{r}}\frac{1}{2}\sum_{a,b=0}^{3}\phi^{(a)}(\mathbf{r},t)\,\eta_{ab}\phi^{(b)}(\mathbf{r},t)-i\ln\det[i\partial_t+\mu-M(\phi)]. \tag{2.18}$$

Here we define the matrix element of $M(\phi)$ by

$$\langle\mathbf{r},t,\sigma|M(\phi)|\mathbf{r}',t',\sigma'\rangle=-t\sum_{j=x,y}\delta_{\sigma,\sigma'}\delta_{\mathbf{r}',\mathbf{r}\pm\mathbf{e}_j}\delta(t-t')-\frac{\sqrt{U}}{2}\sum_{a,b}\eta_{ab}\phi^{(a)}(\mathbf{r},t)\times\tau^{(b)}_{\sigma\sigma'}\delta_{\mathbf{r},\mathbf{r}'}\delta(t-t'). \tag{2.19}$$

And using the relation $\ln\det\mathbf{A}=\mathrm{tr}\ln\mathbf{A}$ that holds for an arbitrary operator $\mathbf{A}$ we obtain

$$S_{\text{eff}}(\phi)=\int dt\sum_{\mathbf{r}}\frac{1}{2}\sum_{a,b=0}^{3}\phi^{(a)}(\mathbf{r},t)\,\eta_{ab}\phi^{(b)}(\mathbf{r},t)-i\,\mathrm{tr}\{\ln[i\partial_t+\mu-M(\phi)]\}. \tag{2.20}$$

III. FERMION AND BOSON GREEN'S FUNCTIONS

The discussion of the previous section is quite general. By choosing a boson field that represents a suitable space configuration corresponding to some ordered state one can discuss a chosen magnetic state.[23] In this paper we restrict our discussion to the case of the paramagnetic state. Investigation on the antiferromagnetic state has already been performed using the same formulation by one of the authors[25] and detailed results will be presented in another publication.

At first we derive the saddle-point solution of the effective action (2.20) in the paramagnetic states. From Eq. (2.20) we obtain the following saddle point (mean-field) equation:

$$\frac{\delta S_{\text{eff}}}{\delta\phi^{(a)}(\mathbf{r},t)}=\eta_{aa}\phi^{(a)}_0(\mathbf{r},t)-i\,\mathrm{tr}\left[\frac{-1}{i\partial_t+\mu-M(\phi_0)}\frac{\delta M(\phi)}{\delta\phi^{(a)}(\mathbf{r},t)}\right]=0. \tag{3.1}$$

For each a, we have the solution

$$\phi^{(a)}_0(\mathbf{r},t)=\sqrt{U}\sum_{\sigma,\sigma'}iG_{\sigma\sigma'}(\mathbf{r},t;\mathbf{r},t;\phi_0)\frac{\tau^{(a)}_{\sigma'\sigma}}{2}. \tag{3.2}$$

Here we have a defined single-electron Green's function by

$$G_{\sigma\sigma'}(\mathbf{r},t;\mathbf{r}',t';\phi)\equiv\langle\mathbf{r},t,\sigma|\left(\frac{1}{i\partial_t+\mu-M(\phi)}\right)|\mathbf{r}',t',\sigma'\rangle \tag{3.3}$$

and $G_{\sigma\sigma'}(\mathbf{r},t;\mathbf{r}',t';\phi_0)$ is the mean-field Green's function. Using the relation

$$\langle s^{(a)}(\mathbf{r},t)\rangle=-i\sum_{\sigma,\sigma'}G_{\sigma\sigma'}(\mathbf{r},t;\mathbf{r},t;\phi_0)\frac{\tau^{(a)}_{\sigma'\sigma}}{2}, \tag{3.4}$$

we obtain

$$\phi^{(a)}_0(\mathbf{r},t)=-\sqrt{U}\langle s^{(a)}(\mathbf{r},t)\rangle. \tag{3.5}$$

Since we consider the system in the paramagnetic state, $\langle s^{(0)}(\mathbf{r},t)\rangle\neq 0$ holds for $a=0$ and $\langle s^{(a)}(\mathbf{r},t)\rangle=0$ for $a=1,2,3$. Thus, the saddle-point values of boson fields are $\phi^{(0)}_0=-\sqrt{U}n/2$ for $a=0$ and $\phi^{(a)}_0=0$ for $a=1,2,3$.

In the $(\mathbf{k},\omega)$ representation the mean-field Green's function can be written as

$$G_0(\mathbf{k},\omega)=\frac{1}{\omega+\mu-[\varepsilon_{\mathbf{k}}+(U/4)n]+i\eta\mathrm{sgn}(\omega)}, \quad (3.6)$$

where $\varepsilon_{\mathbf{k}}=-2t(\cos k_x+\cos k_y)$ is the energy dispersion of the tight-binding model on the two-dimensional square lattice. The symbol ''sgn'' means the sign function. The mean-field Green's function is just the noninteracting Green's function with the single-particle energy shifted by $Un/4$. That is similar to the usual Hartree-Fock approximation. The factor $U/4$ originates from the form of our starting expression of the interacting Hamiltonian H' of Eq. (2.7). This form is particularly suitable to consider electrons in the strong interaction regime although the conventional form is perhaps more useful to calculate the total ground-state electronic energy of the system. For simplicity we introduce the chemical potential μ_0 in the mean-field approximation as $\mu_0=\mu-Un/4$. Then we have

$$G_0(\mathbf{k},\omega)=\frac{1}{\omega+\mu_0-\varepsilon_{\mathbf{k}}+i\eta\mathrm{sgn}(\omega)}. \quad (3.7)$$

Such redefinition of the chemical potential does not affect the electronic states of the system. We determine the chemical potential μ_0 to be consistent with the electron number conservation. The electron number n per a lattice site is given by

$$n=\sum_{\mathbf{k},\sigma}\theta(\mu_0-\varepsilon_{\mathbf{k}}) \quad (3.8)$$

at zero temperature. By solving this for fixed n we get the chemical potential μ_0 for specified doping $\delta=1-n$. Electronic states in the saddle-point approximation are trivial.

Next we take into account the fluctuations of bosons around the saddle point. To this end we replace the boson fields ϕ by a sum of mean-field part ϕ_0 and fluctuation part $\delta\phi$. Then we have $M(\phi)=M(\phi_0)+\delta M(\delta\phi)$. In the effective action S_{eff} (2.20) we can rewrite the logarithm in the trace of the last term as

$$\begin{aligned}&\ln[i\partial_t+\mu-M(\phi_0)-\delta M(\delta\phi)]\\&\quad=\ln\{[i\partial_t+\mu-M(\phi_0)][1-\hat{G}(\phi_0)\delta M(\delta\phi)]\}\\&\quad=\ln[i\partial_t+\mu-M(\phi_0)]+\ln[1-\hat{G}(\phi_0)\delta M(\delta\phi)] \quad (3.9)\end{aligned}$$

with

$$\hat{G}(\phi_0)=[i\partial_t+\mu-M(\phi_0)]^{-1} \quad (3.10)$$

and the matrix element of $\delta M(\delta\phi)$ is given by

$$\begin{aligned}\langle\mathbf{r},t,\sigma|\,\delta M(\delta\phi)|\mathbf{r}',t',\sigma'\rangle=&-\frac{\sqrt{U}}{2}\sum_{a,b}\eta_{ab}\delta\phi^{(a)}(\mathbf{r},t)\\&\times\tau^{(b)}_{\sigma\sigma'}\delta_{\mathbf{r},\mathbf{r}'}\delta(t-t'). \quad (3.11)\end{aligned}$$

By expanding the last term of Eq. (3.9) as

$$\ln[1-\hat{G}(\phi_0)\delta M(\delta\phi)]=-\sum_{n=1}^{\infty}\frac{1}{n}[\hat{G}(\phi_0)\delta M(\delta\phi)]^n, \quad (3.12)$$

we obtain an expansion expression of the effective action S_{eff}

$$S_{\mathrm{eff}}=S_0+S_1+S_2+\cdots, \quad (3.13)$$

where S_n is the nth-order fluctuation term. S_0 is a mean-field contribution and since S_1 involves only a single fluctuation, it vanishes identically. The second-order term can be written as

$$\begin{aligned}S_2=&\int dt\sum_{\mathbf{r}}\frac{1}{2}\sum_{a,b=0}^{3}\delta\phi^{(a)}(\mathbf{r},t)\eta_{ab}\delta\phi^{(b)}(\mathbf{r},t)\\&+i\mathrm{tr}\{\tfrac{1}{2}[\hat{G}(\phi_0)\delta M(\delta\phi)]^2\}. \quad (3.14)\end{aligned}$$

Using Eq. (3.11) and the definition of η_{ab}, we obtain that

$$\begin{aligned}S_2=&\int dt\sum_{\mathbf{r},a}\frac{1}{2}\delta\phi^{(a)}(\mathbf{r},t)\eta_{aa}\delta\phi^{(a)}(\mathbf{r},t)\\&+\frac{i}{2}\sum_{a,a'}\eta_{aa}\eta_{a'a'}U\int dt_1\sum_{\mathbf{r}_1}\int dt\\&\times\sum_{\mathbf{r}}\sum_{\sigma,\sigma_1,\sigma_2,\sigma_3}G_{\sigma\sigma_1}(\mathbf{r},t;\mathbf{r}_1,t_1;\phi_0)\frac{\tau^{(a)}_{\sigma_1\sigma_2}}{2}\\&\times G_{\sigma_2\sigma_3}(\mathbf{r}_1,t_1;\mathbf{r},t;\phi_0)\frac{\tau^{(a')}_{\sigma_3\sigma}}{2}\delta\phi^{(a)}(\mathbf{r}_1,t_1)\delta\phi^{(a')}(\mathbf{r},t). \quad (3.15)\end{aligned}$$

By a Fourier transformation we then have

$$S_2=\sum_a\sum_{\mathbf{q}}\int\frac{d\nu}{2\pi}\frac{1}{2}\delta\phi^{*(a)}(\mathbf{q},\nu)D_{aa}(\mathbf{q},\nu)^{-1}\delta\phi^{(a)}(\mathbf{q},\nu) \quad (3.16)$$

where $D_{aa}(\mathbf{q},\nu)$ is the boson propagator given by

$$D_{aa}(\mathbf{q},\nu)=\frac{1}{\eta_{aa}+(U/2)\chi_0(\mathbf{q},\nu)} \quad (3.17)$$

and the electron-hole polarization function $\chi_0(\mathbf{q},\nu)$ is defined by

$$\chi_0(\mathbf{q},\nu)=i\sum_{\mathbf{k}}\int\frac{d\omega}{2\pi}G_0(\mathbf{k},\omega)G_0(\mathbf{k}+\mathbf{q},\omega+\nu). \quad (3.18)$$

Figure 1(a) shows the diagram that represents $\chi_0(\mathbf{q},\nu)$.

To make the following discussion clear, here we change the notation of the boson propagators into D_c for the charge-boson propagator D_{00} and D_s for the spin-boson propagators D_{aa} for $a=1,2,3$. At the same time we introduce $\eta_c=1$ and $\eta_s=-1$ instead of η_{aa}. As a result, the boson propagator is written as

$$D_\alpha(\mathbf{q},\nu)=\frac{1}{\eta_\alpha+(U/2)\chi_0(\mathbf{q},\nu)}, \quad (3.19)$$

where the subscript α takes c or s.

The denominator of the D_s has a pole in some value of U for a fixed electron number n and the divergence due to

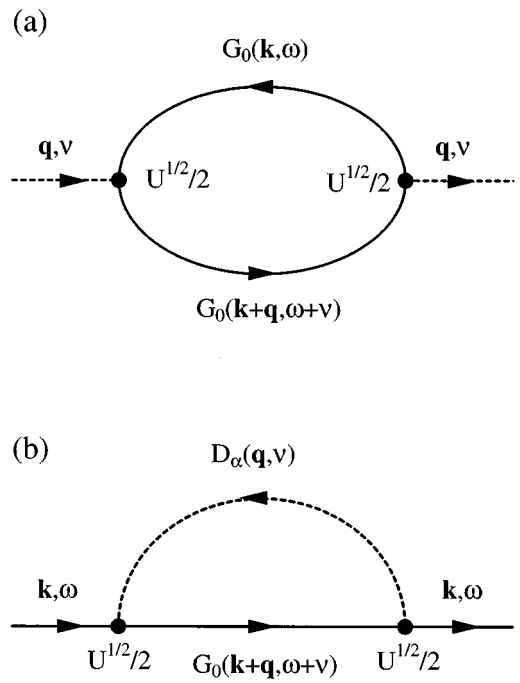

FIG. 1. One-loop Feynman diagrams that represent (a) the mean-field polarization function $\chi_0(\mathbf{q},\nu)$ and (b) the fermion self-energy $\Sigma(\mathbf{k},\omega)$. The solid line represents the mean-field fermion Green's function $G(\mathbf{k},\omega)$. The dashed line represents the boson propagator $D_\alpha(\mathbf{q},\nu)$.

the pole relates to a magnetic instability of the paramagnetic system. It is an important point that, in the present treatment, the Stoner condition becomes $1=(U/2)\mathrm{Re}\chi_0(\mathbf{q},0)$. In ordinary random-phase approximation (RPA) based on the U perturbation theory the condition is given by $1=U\mathrm{Re}\chi_0(\mathbf{q},0)$.[22] The Stoner criterion in our case is weaker than the usual one and this works as an advantage in our calculation.

The interacting fermion Green's function beyond the mean-field approximation is calculated by expanding the expression of the definition of the Green's function given by Eq. (3.3):

$$\begin{aligned}\hat{G}(\phi)^{-1}&=i\partial_t+\mu-M(\phi_0)-\delta M(\delta\phi)\\&=\hat{G}^{-1}(\phi_0)-\delta M(\delta\phi_0)\\&=\hat{G}^{-1}(\phi_0)\{1-\hat{G}(\phi_0)\delta M(\delta\phi)\}\end{aligned}\tag{3.20}$$

and

$$\begin{aligned}\hat{G}(\phi)&=\{1-\hat{G}(\phi_0)\delta M(\delta\phi)\}^{-1}\hat{G}(\phi_0)\\&=\sum_{n=0}^{\infty}\{\hat{G}(\phi_0)\delta M(\delta\phi)\}^n\hat{G}(\phi_0).\end{aligned}\tag{3.21}$$

Since we have introduced auxiliary boson fields, our Hilbert space has been enlarged and it consists of the original fermion space and the auxiliary boson space. From the physical meaning of the boson fluctuations, we introduce the relation that $\langle\mathrm{Gnd}|\delta\phi|\mathrm{Gnd}\rangle=0$ with $|\mathrm{Gnd}\rangle$ being a boson ground state in the enlarged Hilbert space. By this relation, we see that the odd-order terms in the expansion series Eq. (3.21) vanish. Then, we can write the series as the summation of the even-order terms:

$$\hat{G}(\phi)=\sum_{n=0}^{\infty}\{\hat{G}(\phi_0)\delta M(\delta\phi)\}^{2n}\hat{G}(\phi_0).\tag{3.22}$$

From the definition of the fermion Green's function, the term of the second order in $\delta\phi$ of Eq. (3.22) becomes

$$\langle\mathbf{r},t,\sigma|\hat{G}_{(2)}(\phi)|\mathbf{r}',t',\sigma'\rangle=\langle\mathbf{r},t,\sigma|\hat{G}(\phi_0)\delta M(\delta\phi)\hat{G}(\phi_0)\delta M(\delta\phi)\hat{G}(\phi_0)|\mathbf{r}',t',\sigma'\rangle.\tag{3.23}$$

Using the relation

$$\sum_\sigma\int dt\sum_{\mathbf{r}}|\mathbf{r},t,\sigma\rangle\langle\mathbf{r},t,\sigma|=1\tag{3.24}$$

and also Eqs. (3.7) and (3.11), the second-order Green's function is written as

$$i\sum_{\sigma''}\int dt_1dt_2\sum_{\mathbf{r}_1,\mathbf{r}_2}\frac{U}{4}G(\mathbf{r},t;\mathbf{r}_1,t_1;\phi_0)G(\mathbf{r}_1,t_1;\mathbf{r}_2,t_2;\phi_0)G(\mathbf{r}_2,t_2;\mathbf{r}',t';\phi_0)\sum_{a=0}^{3}\tau^{(a)}_{\sigma\sigma''}\tau^{(a)}_{\sigma''\sigma'}D_{aa}(\mathbf{r}_2,t_2;\mathbf{r}_1,t_1),\tag{3.25}$$

where we have defined the boson propagator as

$$D_{ab}(\mathbf{r},t;\mathbf{r}',t')=-i\langle\mathrm{Gnd}|\delta\phi^{(a)}(\mathbf{r},t)\delta\phi^{(b)}(\mathbf{r}',t')|\mathrm{Gnd}\rangle.\tag{3.26}$$

We can assume that the expression of the boson propagator is the same as the one already given by Eq. (3.19). After Fourier transformation, we have

$$iG_0(\mathbf{k},\omega)\frac{U}{4}\sum_{a=0}^{3}\sum_{\mathbf{q}}\int\frac{d\nu}{2\pi}G_0(\mathbf{k}+\mathbf{q},\omega+\nu)D_{aa}(\mathbf{q},\nu)G_0(\mathbf{k},\omega).\tag{3.27}$$

The second-order Green's function has the one-loop fermion-boson bubble self-energy. By calculating higher-order terms in the same way, we can derive arbitrary order of the Green's function with a corresponding self-energy including a vertex correction. In this work we consider the partial summation of the Green's function including only the one-loop fermion-boson bubble. Neglecting vertex corrections at this stage, we have the following Dyson equation of the fermion Green's function.

$$G(\mathbf{k},\omega)^{-1}=G_0(\mathbf{k},\omega)^{-1}-\Sigma(\mathbf{k},\omega), \tag{3.28}$$

$$\Sigma(\mathbf{k},\omega)=\Sigma_c(\mathbf{k},\omega)+3\Sigma_s(\mathbf{k},\omega), \tag{3.29}$$

where the fermion self-energies are written as

$$\Sigma_\alpha(\mathbf{k},\omega)=i\frac{U}{4}\sum_{\mathbf{q}}\int\frac{d\nu}{2\pi}G_0(\mathbf{k}+\mathbf{q},\omega+\nu)D_\alpha(\mathbf{q},\nu), \tag{3.30}$$

where $\alpha=c,s$ for the charge and spin components, respectively. The corresponding Feynman diagram is shown in Fig. 1(b).

IV. FERMION SELF-ENERGIES AND SPECTRA OF THE BOSON PROPAGATORS

In this section we show the results of our numerical analysis of the fermion self-energies. The real and imaginary parts of the fermion self-energies for both charge and spin components are obtained from Eq. (3.30). By substituting Eq. (3.7) into Eq. (3.30) and performing the ν integral, we obtain the imaginary part of the self-energy in the following form:

$$\begin{aligned}\mathrm{Im}\Sigma_\alpha(\mathbf{k},\omega)=-\frac{U}{8}\sum_{\mathbf{q}}&[\mathrm{sgn}(\varepsilon_{\mathbf{k}+\mathbf{q}}-\mu_0-\omega)\\&-\mathrm{sgn}(\varepsilon_{\mathbf{k}+\mathbf{q}}-\mu_0)]\\&\times\mathrm{Im}D_\alpha(\mathbf{q},\varepsilon_{\mathbf{k}+\mathbf{q}}-\mu_0-\omega),\end{aligned} \tag{4.1}$$

where $\alpha=s,c$ correspond to the spin and charge fluctuations, respectively. If we have $\mathrm{Im}\Sigma_\alpha(\mathbf{k},\omega)$, the real part of the fermion self-energy is obtained by the Kramers-Kronig transformation,

$$\mathrm{Re}\Sigma_\alpha(\mathbf{k},\omega)=\frac{\mathrm{P}}{\pi}\int d\omega'\,\frac{\mathrm{sgn}\omega'\,\mathrm{Im}\Sigma_\alpha(\mathbf{k},\omega')}{\omega'-\omega}. \tag{4.2}$$

As we easily see from the expression of the fermion self-energy, the behavior of the boson spectrum $\mathrm{Im}D_\alpha$ is a determinant for the fermion self-energies. From Eq. (3.19), $\mathrm{Im}D_\alpha$ is given by

$$\mathrm{Im}D_\alpha(\mathbf{q},\nu)=\frac{-(U/2)\mathrm{Im}\chi_0(\mathbf{q},\nu)}{[1+\eta_\alpha(U/2)\mathrm{Re}\chi_0(\mathbf{q},\nu)]^2+[(U/2)\mathrm{Im}\chi_0(\mathbf{q},\nu)]^2}. \tag{4.3}$$

The imaginary part of the polarization function $\chi_0(\mathbf{q},\nu)$ is calculated from Eq. (3.18) using the mean-field Green's function Eq. (3.7). We have that

$$\begin{aligned}\mathrm{Im}\chi_0(\mathbf{q},\nu)=\pi\,\mathrm{sgn}(\nu)\sum_{\mathbf{k}}&[\theta(\varepsilon_{\mathbf{k}+\mathbf{q}}-\mu_0)-\theta(\varepsilon_{\mathbf{k}}-\mu_0)]\\&\times\delta(\nu-\varepsilon_{\mathbf{k}+\mathbf{q}}+\varepsilon_{\mathbf{k}}).\end{aligned} \tag{4.4}$$

We calculated this formula numerically using the technique explained in the Appendix. The real part of $\chi_0(\mathbf{q},\nu)$ is again obtained from the Kramers-Kronig relation as

$$\begin{aligned}\mathrm{Re}\chi_0(\mathbf{q},\nu)&=\frac{\mathrm{P}}{\pi}\int d\nu'\,\frac{\mathrm{sgn}(\nu')\mathrm{Im}\chi_0(\mathbf{q},\nu')}{\nu'-\nu}\\&=\sum_{\mathbf{k}}\frac{\theta(\varepsilon_{\mathbf{k}}-\mu_0)-\theta(\varepsilon_{\mathbf{k}+\mathbf{q}}-\mu_0)}{\nu-\varepsilon_{\mathbf{k}+\mathbf{q}}+\varepsilon_{\mathbf{k}}}.\end{aligned} \tag{4.5}$$

In Fig. 2 we show the low-energy behavior of the boson spectral functions calculated for $U/t=3.0$ and 6.0 and for several wave vector $\mathbf{q}$'s at hole doping $\delta=0.2$. For this doping concentration, the critical U evaluated from the Stoner condition is $U_{\mathrm{cr}}/t=6.3$. In the present approximation the energy range, in which the boson spectrum is meaningful, is the same as that of the particle-hole individual excitation obtained from the mean-field fermion bubble diagram. As is well known, if we consider the doped system, the single excitations have a gap in the region $\mathbf{q}>2\mathbf{k}_F$ around zero excitation energy. In the case of the two-dimensional Hubbard model, the maximum value of the gap is $2|\mu_0|$ at $\mathbf{q}=(\pi,\pi)$. For hole doping $\delta=0.2$, the Fermi momentum $\mathbf{k}_F$ in the (1,1) direction becomes $\mathbf{k}_F/\pi=(0.47,0.47)$ and the corresponding chemical potential is $\mu_0=-0.43$. In the inset of Fig. 2 the gap is observed in our data as expected.

For the change of the value of the Coulomb interaction from $U/t=3.0$ to $U/t=6.0$, the charge boson spectra have no significant change. It behaves linearly by energy and the $\mathbf{q}$ dependence is also weak. On the other hand, the spin-boson spectrum shows a drastic change as U/t approaches the critical value determined by the Stoner condition. Near $\mathbf{q}=2\mathbf{k}_F$, the spin-boson spectrum has a strong enhancement, which corresponds to the paramagnon excitation[26] that characterizes the onset of the magnetic instability. Contrary to this, at small $\mathbf{q}$, there is no sign of enhancement. For small dopings, such a strong enhancement in the spin excitation takes place near $\mathbf{q}=(\pi,\pi)$ and it implies that the system is close to the antiferromagnetic instability.

In the gap of the spin-boson spectral function for $\mathbf{q}>2\mathbf{k}_F$ there exists another structure for a certain range of the Coulomb interaction. This can be understood as follows. Because of the rapid drop of $\mathrm{Im}\chi_0(\mathbf{q},\nu)$ near the gap, $\mathrm{Re}\chi_0(\mathbf{q},\nu)$ has a peak structure near the low-energy edge of the individual excitation. When the peak maximum is at $(\mathbf{q}_c,\nu_c)$, if U becomes large enough to satisfy the condition $\mathrm{Re}\chi_0(\mathbf{q}_c,\nu_c)>2/U>\mathrm{Re}\chi_0(\mathbf{q}_S,0)$ with $\mathbf{q}_S$ being the wave vector for the critical point of the Stoner condition, the real part of the denominator of $\mathrm{Im}D_s$ has two poles. Because of this, the spin excitation has two peaks with one of them inside the gap. This means that the paramagnon peak is split into two peaks by the Coulomb interaction. This paramagnon split seems to be a precursor phenomenon of the antiferromagnetic instability in the doped two-dimensional Hubbard

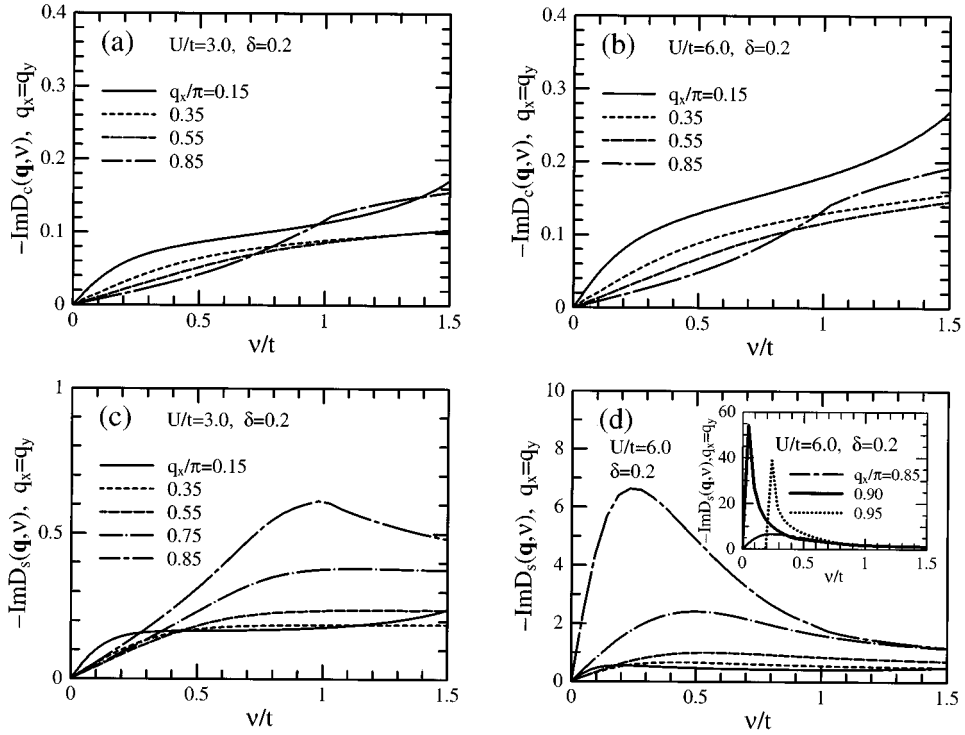

FIG. 2. Low-energy behavior of the boson spectral functions calculated for several $\mathbf{q}$'s in the (1,1) direction ($q_x=q_y$) at $\delta=0.2$: the charge-boson spectra $\mathrm{Im}D_c(\mathbf{q},\nu)$ for (a) $U/t=3.0$ and for (b) $U/t=6.0$; the spin-boson spectra $\mathrm{Im}D_s(\mathbf{q},\nu)$ for (c) $U/t=3.0$ and for (d) $U/t=6.0$. The inset in (d) shows the sharp peak of $\mathrm{Im}D_s(\mathbf{q},\nu)$ for large $\mathbf{q}$ close to $\mathbf{q}=(\pi,\pi)$. For $q_x/\pi(=q_y/\pi)=0.95$, the gap (see the text) is observed. Note the difference of the scale of the intensity in these figures.

model. A similar behavior to this exists in the parabolic band model and also in models with dimension higher than two. The paramagnon split has a resemblance to the appearance of the zero sound mode. Within the RPA, the paramagnon split appears in the magnetic susceptibility while the zero sound mode is manifest in the charge susceptibility. Note that the paramagnon split is not a Goldstone mode and the same goes for the spin sound mode.[27] In the present approximation the paramagnon split has a δ-function structure. However, the excitation peak should be weaker than that if we take into account higher-order contribution to the self-energies of fermions or if we solve the Dyson equation self-consistently. In our numerical calculation of the fermion self-energy we considered the paramagnon-split structure in the spin-fluctuation boson spectral function assuming that it has a Lorenzian form with a width of the order of an integral unit of the numerical integration.

Using Eqs. (4.1)–(4.5), we calculated the fermion self-energy at $\delta=0.2$ for $U/t=3.0$ and $U/t=6.0$ and obtained the following results. We compare the charge component Σ_c and the spin component Σ_s of the real and imaginary parts of the self-energy at $\mathbf{k}=(\pi/2,\pi/2)$ in Fig. 3. For small U ($U/t=3.0$), the difference of the charge and the spin components is not remarkable. For large U ($U/t=6.0$), clear differences between them appears in both the imaginary part and the real part of the self-energies. The difference is caused by the effect of strong enhancement of the paramagnon peak that appears in $\mathrm{Im}D_s$ in the low boson-energy region near $\mathbf{q}=2\mathbf{k}_F$. The most important point in the behavior of the imaginary part of the self-energy concerns perhaps their low-energy limits. For large U and energy range around $\omega=0$, $\mathrm{Im}\Sigma_c$ shows the Fermi-liquid-like ω^2 behavior. In contrast, $\mathrm{Im}\Sigma_s$ behaves linearly in ω. This implies that the charge fluctuations persists with Fermi-liquid properties while the spin fluctuation acts to break the Fermi-liquid regime.

These energy dependences of the imaginary part of the fermion self-energy can be understood by analyzing the $\mathbf{q}$ summation in Eq. (4.1). Firstly, we change the $\mathbf{q}$ summation into a $\mathbf{q}$ integral,

$$\mathrm{Im}\Sigma_\alpha(\mathbf{k},\omega)=-\frac{U}{8}\int\frac{d\mathbf{q}}{(2\pi)^2}[\mathrm{sgn}(\varepsilon_{\mathbf{k}+\mathbf{q}}-\mu_0-\omega)-\mathrm{sgn}(\varepsilon_{\mathbf{k}+\mathbf{q}}-\mu_0)]\mathrm{Im}D_\alpha(\mathbf{q},\varepsilon_{\mathbf{k}+\mathbf{q}}-\mu_0-\omega). \tag{4.6}$$

The contribution to the integral comes from the region satisfying $\mathrm{sgn}(\varepsilon_{\mathbf{k}+\mathbf{q}}-\mu_0-\omega)-\mathrm{sgn}(\varepsilon_{\mathbf{k}+\mathbf{q}}-\mu_0)\neq 0$ and $\mathrm{Im}D_\alpha(\mathbf{q},\varepsilon_{\mathbf{k}+\mathbf{q}}-\mu_0-\omega)\neq 0$, for some given values of $\mathbf{k}$ and ω. $\mathrm{Im}D_\alpha(\mathbf{q},\omega)$ has a finite value in the region corresponding to particle-hole excitations. If we consider $\omega>0$, from the restriction of the sign function, we find two conditions; one is the restriction of the boson energy ν written as $\nu=\varepsilon_{\mathbf{k}+\mathbf{q}}-\mu_0-\omega<0$ and the other is $\varepsilon_{\mathbf{k}+\mathbf{q}}-\mu_0>0$. In Fig. 4, we schematically plot these conditions in the $(\mathbf{q},\nu)$ space for $\mathbf{k}=\mathbf{k}_F$ where $\mathbf{k}_F/\pi=(0.35,0.35)$. For simplicity, we consider only the (1,1) direction of $\mathbf{q}$. In the region surrounded by dashed lines $\mathrm{Im}D_\alpha(\mathbf{q},\nu)$ has a finite value. The dotted line represents $\varepsilon_{\mathbf{k}_F+\mathbf{q}}-\mu_0$. For $\omega=2.0$ and 5.0, $\nu=\varepsilon_{\mathbf{k}_F+\mathbf{q}}-\mu_0-\omega$ are drawn as solid curves. The thick parts of the solid curves give the valid ranges of $\mathrm{Im}D_\alpha(\mathbf{q},\nu)$ to the $\mathbf{q}$ integration of $\mathrm{Im}\Sigma_\alpha(\mathbf{k},\omega)$. From the figure, we see that for small ω and for $\mathbf{k}$ near $\mathbf{k}_F$, the important contribution to the imaginary part of the self-energy comes from the low-energy regions of $\mathrm{Im}D_\alpha(\mathbf{q},\nu)$ near $\mathbf{q}\sim-2\mathbf{k}_F$ and $\mathbf{q}\sim 0$.

In the following, using the above analysis and the behavior of the calculated boson spectra, we roughly evaluate the low-energy behavior of the charge and spin components of the imaginary part of the self-energy. From the results of the calculation of the energy dependence of both the charge- and

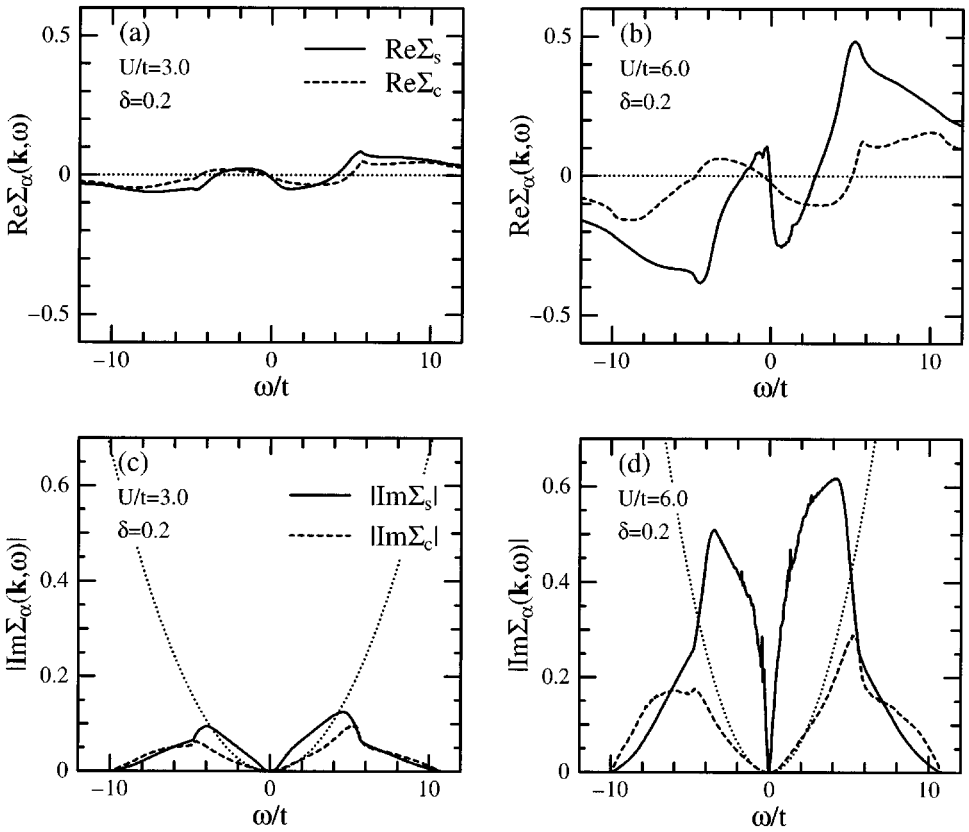

FIG. 3. Energy ω/t dependence of the spin (solid line) and charge (dashed line) components of the fermion self-energy at $\mathbf{k}=(\pi/2,\pi/2)$ for doping $\delta=0.2$: the real parts for (a) $U/t=3.0$ and for (b) $U/t=6.0$; the imaginary parts for (c) $U/t=3.0$ and for (d) $U/t=6.0$. Dotted curves in (c) and (d) represent the approximate form of $\mathrm{Im}\Sigma_c(\mathbf{k},\omega)$ (see the text) using $\rho(\mu_0)=0.18$, (c) $A_c=0.10$, and (d) $A_c=0.12$.

spin-boson propagator spectra, we find that both spectra are proportional to ν for small ν, and the $\mathrm{Im}D_c$ depends weakly on $\mathbf{q}$, contrary to $\mathrm{Im}D_s$, which has a sharp enhancement at $\mathbf{q}=2\mathbf{k}_F$. Since the boson propagator is a symmetrical function of $\mathbf{q}$, the sharp paramagnon enhancement appears also at the $\mathbf{q}=-2\mathbf{k}_F$. Then, we assume the following forms of the boson spectra for small ν:

$$\mathrm{Im}D_c(\mathbf{q},\nu)\sim -A_c(\mathbf{q})|\nu| \tag{4.7}$$

and

$$\mathrm{Im}D_s(\mathbf{q},\nu)\sim -\tilde{\delta}_{\mathbf{q},-2\mathbf{k}_F}A_s(2\mathbf{k}_F)|\nu|, \tag{4.8}$$

where A_c and A_s are $\mathbf{q}$-dependent positive factors for the charge and spin excitations, respectively, and to take some account of broadening effects we have introduced $\tilde{\delta}_{\mathbf{q},-2\mathbf{k}_F}$, which is equal to 1 for $\mathbf{q}$ around $-2\mathbf{k}_F$ and is 0 for other values of $\mathbf{q}$. Using the relation $\mathrm{sgn}(x)=2\theta(x)-1$ in Eq. (4.6), we have

$$\mathrm{Im}\Sigma_\alpha(\mathbf{k},\omega)=-\frac{U}{4}\int\frac{d\mathbf{q}}{(2\pi)^2}[\theta(\varepsilon_{\mathbf{k}+\mathbf{q}}-\mu_0-\omega)-\theta(\varepsilon_{\mathbf{k}+\mathbf{q}}-\mu_0)]\mathrm{Im}D_\alpha(\mathbf{q},\varepsilon_{\mathbf{k}+\mathbf{q}}-\mu_0-\omega). \tag{4.9}$$

For the charge components, from the weak $\mathbf{q}$ dependence of $\mathrm{Im}D_c(\mathbf{q},\nu)$, we take $A_c(\mathbf{q})\sim A_c=\mathrm{const}$. Using this and the above assumption, we obtain

$$\mathrm{Im}\Sigma_c(\mathbf{k},\omega)\sim\frac{U}{4}\int\frac{d\mathbf{q}}{(2\pi)^2}[\theta(\varepsilon_{\mathbf{k}+\mathbf{q}}-\mu_0-\omega)-\theta(\varepsilon_{\mathbf{k}+\mathbf{q}}-\mu_0)]A_c|\varepsilon_{\mathbf{k}+\mathbf{q}}-\mu_0-\omega|. \tag{4.10}$$

By changing the variable $\mathbf{q}$ to $\mathbf{q}-\mathbf{k}$ in the $\mathbf{q}$ integral, we have

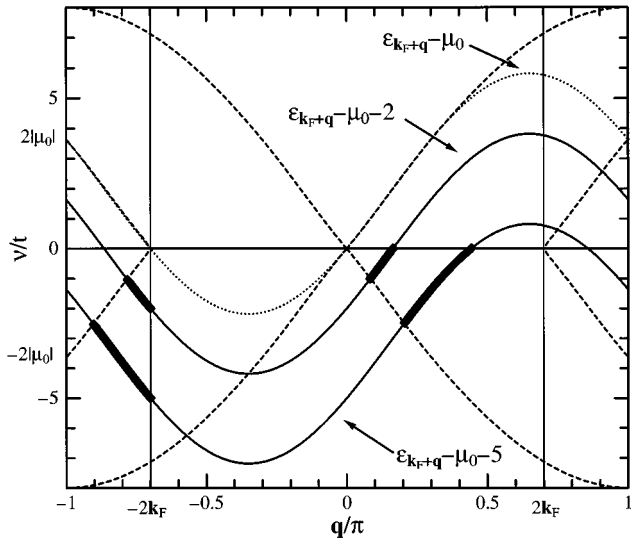

FIG. 4. Schematic explanation of the contribution range to the $\mathbf{q}$ integral of the imaginary part of the self-energy $\mathrm{Im}\Sigma_\alpha(\mathbf{k},\omega)$. The area surrounded by the dashed line represents the meaningful region of the individual excitation and also of $\mathrm{Im}D_\alpha(\mathbf{q},\nu)$. The dotted line is $\varepsilon_{\mathbf{k}_F+\mathbf{q}}-\mu_0$. The solid curves correspond to $\nu=\varepsilon_{\mathbf{k}_F+\mathbf{q}}-\mu_0-\omega$ for $\omega=2.0$ and for $\omega=5.0$. The thick parts of the solid curves represent the contribution range to the $\mathbf{q}$ integral. For explanation, a large value of μ_0 [$\mu_0=-1.82$, $\mathbf{k}_F/\pi=(0.35,0.35)$] has been used in this figure.

$$\mathrm{Im}\Sigma_c(\mathbf{k},\omega)\sim\frac{U}{4}A_c\int\frac{d\mathbf{q}}{(2\pi)^2}[\,\theta(\varepsilon_{\mathbf{q}}-\mu_0-\omega)-\theta(\varepsilon_{\mathbf{q}}-\mu_0)]|\varepsilon_{\mathbf{q}}-\mu_0-\omega|. \quad (4.11)$$

This result shows that $\mathrm{Im}\Sigma_c(\mathbf{k},\omega)$ does not depend on $\mathbf{k}$ and it agrees with our numerical result that the charge components of the imaginary part have a weak dependence on $\mathbf{k}$. Furthermore, we can change the above $\mathbf{q}$ integral to the energy integral by introducing the density of states $\rho(\varepsilon)$ of the noninteracting tight-binding band with the band dispersion $\varepsilon_{\mathbf{k}}$. The integration range is the energy region from the band bottom $-4t$ to the band top $4t$ of the noninteracting band. Thus,

$$\mathrm{Im}\Sigma_c(\mathbf{k},\omega)\sim\frac{U}{4}A_c\int_{-4t}^{4t}d\varepsilon\rho(\varepsilon)[\,\theta(\varepsilon-\mu_0-\omega)-\theta(\varepsilon-\mu_0)]|\varepsilon-\mu_0-\omega|. \quad (4.12)$$

By considering the step function we restrict the integration range. For $\omega>0$, using $\varepsilon-\mu_0-\omega<0$ we have

$$\mathrm{Im}\Sigma_c(\mathbf{k},\omega)\sim\frac{U}{4}A_c\int_{\mu_0}^{\mu_0+\omega}d\varepsilon\rho(\varepsilon)\{\varepsilon-(\mu_0+\omega)\}. \quad (4.13)$$

Since our main interest is its behavior around the Fermi energy $\omega=0$, we can approximate $\rho(\varepsilon)$ by $\rho(\mu_0)$ and put it outside of the integral. If we now complete the integration, we find the ω^2 dependence for the charge components of the imaginary part of the self-energy

$$\mathrm{Im}\Sigma_c(\mathbf{k},\omega)\sim-\frac{U}{4}A_c\rho(\mu_0)\omega^2/2. \quad (4.14)$$

By generalizing also for the negative $\omega<0$, finally we have

$$\mathrm{Im}\Sigma_c(\mathbf{k},\omega)\sim-\mathrm{sgn}(\omega)\frac{U}{4}A_c\rho(\mu_0)\omega^2/2. \quad (4.15)$$

Next, we turn to the spin components. By substituting Eq. (4.8) into (4.6) for $\alpha=s$ and $\mathbf{k}=\mathbf{k}_F$, we find

$$\mathrm{Im}\Sigma_s(\mathbf{k}_F,\omega)\sim\frac{U}{4}\int\frac{d\mathbf{q}}{(2\pi)^2}[\,\theta(\varepsilon_{\mathbf{k}_F+\mathbf{q}}-\mu_0-\omega)-\theta(\varepsilon_{\mathbf{k}_F+\mathbf{q}}-\mu_0)]\,\tilde{\delta}_{\mathbf{q},-2\mathbf{k}_F}A_s(2\mathbf{k}_F)\times|\varepsilon_{\mathbf{k}_F+\mathbf{q}}-\mu_0-\omega|. \quad (4.16)$$

For $\omega>0$, $\theta(\varepsilon_{\mathbf{k}_F+\mathbf{q}}-\mu_0-\omega)-\theta(\varepsilon_{\mathbf{k}_F+\mathbf{q}}-\mu_0)$ gives -1 and as discussed above, the main contribution to the integral comes from around $\mathbf{q}=-2\mathbf{k}_F$. Then, we have

$$\mathrm{Im}\Sigma_s(\mathbf{k}_F,\omega)\sim-\frac{U}{4}\Delta A_s(2\mathbf{k}_F)|\varepsilon_{-\mathbf{k}_F}-\mu_0-\omega|, \quad (4.17)$$

where Δ represents the width around $\mathbf{q}=-2\mathbf{k}_F$ in $\mathbf{q}$ space. Using $\varepsilon_{-\mathbf{k}_F}=\mu_0$, we find the linear dependence of $\mathrm{Im}\Sigma_s$,

$$\mathrm{Im}\Sigma_s(\mathbf{k}_F,\omega)\sim-\frac{U}{4}\Delta A_s(2\mathbf{k}_F)\omega. \quad (4.18)$$

For $\omega<0$, we obtain the same expression as this. Note that the above derivation does not apply for $\mathbf{k}$ far form $\mathbf{k}_F$ because the contribution to the $\mathbf{q}$ integral that comes from the other regions is different from in this case and is similar to the case of the charge components. For this, we have that the ω^2 dependence follows for the other location.

We show the above approximate expression of $\mathrm{Im}\Sigma_c(\mathbf{k},\omega)$ as dotted curves in Figs. 3(c) and 3(d). The factor A_c is estimated from the calculated values of $\mathrm{Im}D_c(\mathbf{q},\nu)$. We have chosen $A_c=0.10$ and 0.12 for $U/t=3.0$ and 6.0, respectively, and also $\rho(\mu_0)=0.18$ for the doping $\delta=0.2$. As seen from these figures, the agreement between the explicit calculation and the approximate form is good around $\omega=0$.

We also calculated the total self-energy for several $\mathbf{k}$'s. In Fig. 5 we show the imaginary part of the total self-energy for $U/t=3.0$ (dotted line) and $U/t=6.0$ (solid line). We plot the value divided by U to make the comparison between them easier. In the case of $U/t=6.0$, the $\mathbf{k}$ dependence is characteristic especially around the Fermi energy $\omega=0$. In this case, at the $\mathbf{k}$ points far from the Fermi momentum $\mathbf{k}_F\approx(\pi/2,\pi/2)$, the ω dependence around the Fermi energy resembles the behavior of a Fermi liquid. However, as the position of $\mathbf{k}$ approaches to the Fermi momentum the range of the ω^2-like behavior becomes narrow. Contrary, for $U/t=3.0$, ω^2 behavior holds in a relatively wider range and $\mathbf{k}$ dependence is weak.

We plot also the energy dependence of $\mathrm{Re}\Sigma(\mathbf{k},\omega)-\mu_*$ for several $\mathbf{k}$'s in Fig. 6. For $U/t=6.0$, as the $\mathbf{k}$ approaches the Fermi momentum, the slope of $\mathrm{Re}\Sigma(\mathbf{k},\omega)-\mu_*$ around the Fermi energy becomes large. For $U/t=3.0$ there is not a notable change of slope. The behavior is deeply connected to what happens to the imaginary part.

From all these results we see that the drastic enhancement of the low-energy spin excitation due to strong Coulomb interaction produces the modification of the properties of the Fermi liquid near the Fermi surface.

V. FERMION SPECTRAL FUNCTIONS AND DENSITY OF STATES

The fermion spectral function is obtained from the imaginary part of the single-particle Green's function as

$$A(\mathbf{k},\omega)=-\frac{1}{\pi}\mathrm{sgn}(\omega)\mathrm{Im}G(\mathbf{k},\omega). \quad (5.1)$$

From Eqs. (3.7) and (3.28) we have

$$\mathrm{Im}G(\mathbf{k},\omega)=\frac{\mathrm{Im}\Sigma(\mathbf{k},\omega)}{\{\omega+\mu_*-\varepsilon_{\mathbf{k}}-\mathrm{Re}\Sigma(\mathbf{k},\omega)\}^2+\{\mathrm{Im}\Sigma(\mathbf{k},\omega)\}^2}. \quad (5.2)$$

The chemical potential μ_* contains interaction effects effectively and it has a different value from μ_0 in the mean-field approximation. By calculating the following electron number conservation relation numerically, we can determine the precise value of μ_*:

$$n=2\int_{-\infty}^{0}d\omega N(\omega), \quad (5.3)$$

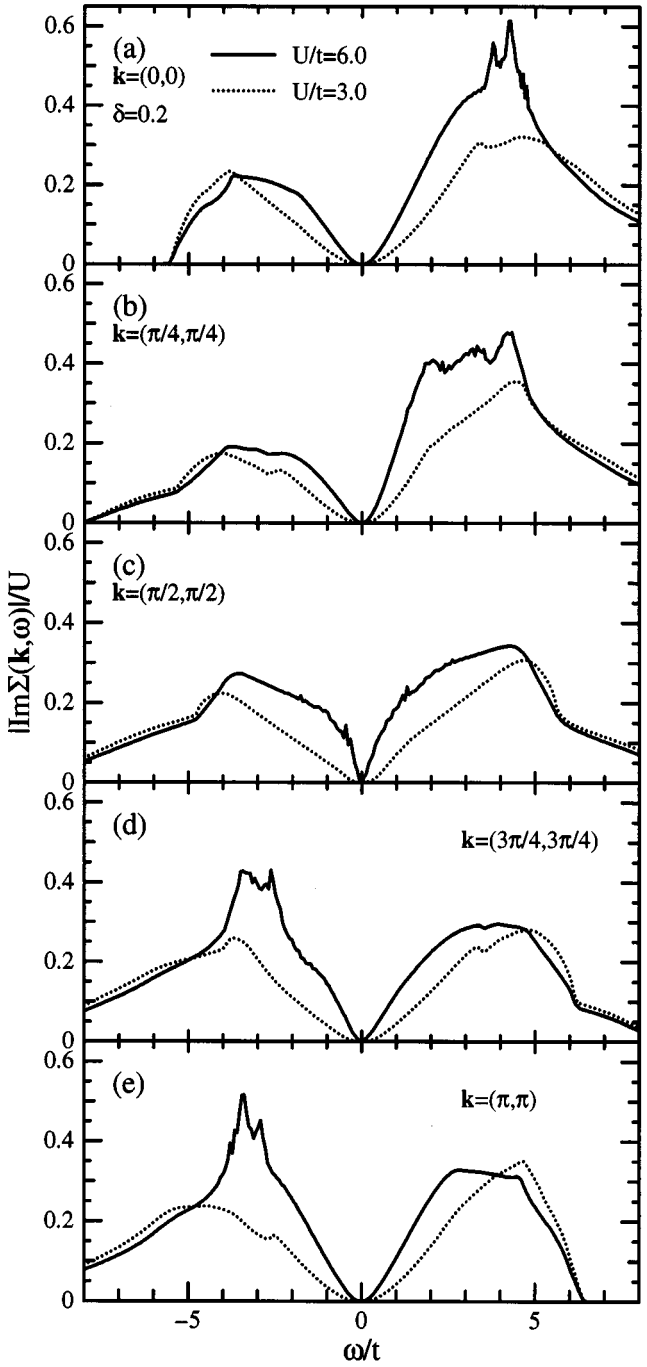

FIG. 5. Energy ω/t dependence of the imaginary part of the total self-energy scaled by U for several $\mathbf{k}$'s at $\delta=0.2$, for $U/t=3.0$ (dotted line) and for $U/t=6.0$ (solid line).

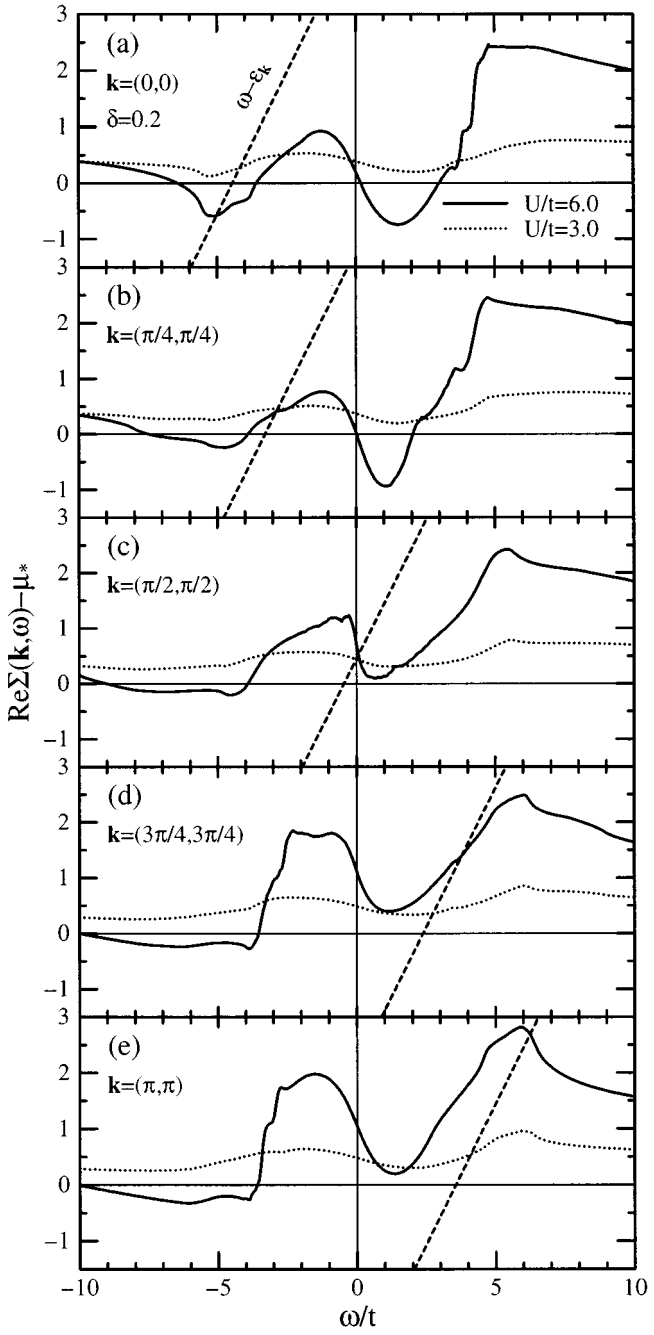

FIG. 6. Energy ω/t dependence of the real part of the total self-energy for several $\mathbf{k}$'s at $\delta=0.2$, for $U/t=3.0$ (dotted line) and for $U/t=6.0$ (solid line). The dashed line represents $\omega-\varepsilon_{\mathbf{k}}$. We plot $\mathrm{Re}\Sigma(\mathbf{k},\omega)-\mu_*$ for the purpose of comparison of the poles of the Green's function for both U's. The calculated values of the chemical potential μ_* are -0.49 for $U/t=3.0$ and -0.92 for $U/t=6.0$.

where the factor 2 is due to spin and $N(\omega)$, the density of states per spin, is defined by

$$N(\omega)=\sum_{\mathbf{k}} A(\mathbf{k},\omega). \tag{5.4}$$

We calculate the density of states performing the summation of the spectral function $A(\mathbf{k},\omega)$ in $\mathbf{k}$ space. In Fig. 7 the evolution of the density of states is shown for several values of the interaction U/t for fixed doping $\delta=0.2$. For $U/t=3.0$ the overall structures of the DOS is almost the same as the noninteracting ($U/t=0.0$) DOS, except for the existence of the band tails, which appear both at the top and at the bottom of the band. As the interaction U becomes large, the band tails are spread out and total bandwidth also become wider. As we will mention in more detail later in the discussion about the spectral function, the development of the band in both positive and negative high-energy regions corresponds to the formation of the upper and the lower

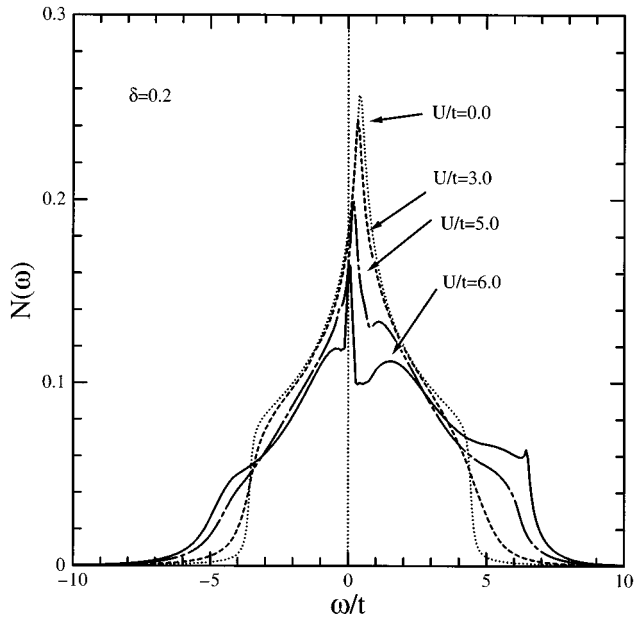

FIG. 7. Density of states at $\delta=0.2$, for $U/t=0.0$ (dotted line), 3.0 (dashed line), 5.0 (dashed-dotted line), and 6.0 (solid line).

Hubbard bands. In the low-energy region there exists a band crossing the Fermi energy $\omega=0$ for all values of U. As U becomes large, the bandwidth becomes narrower. Physically, we recognize that this corresponds to the quasiparticle band in the interacting system as expected on general grounds by the Fermi-liquid theory. For $U/t=5.0$ a pseudo-gap-like structure comes out near $\omega=0.8$. For $U/t=6.0$, the pseudogap becomes wider and, furthermore, another weak dent appears at $\omega=-0.25$. The pseudogap of the DOS in the two-dimensional Hubbard model has already been discussed by Kampf and Schrieffer[28] in the framework of a random-phase approximation. Their approximation scheme for the perturbation theory is perhaps close to our treatment despite the difference in coupling constant and the fact that they considered only the spin fluctuation effects. However, their results differ from ours in one important point. In their approach the pseudogap arises from the negative side of the energy ω and the sharp structure of the quasiparticle band is not observed. The absence of the clear quasiparticle structure in their data might be interpreted as a precursor phenomenon

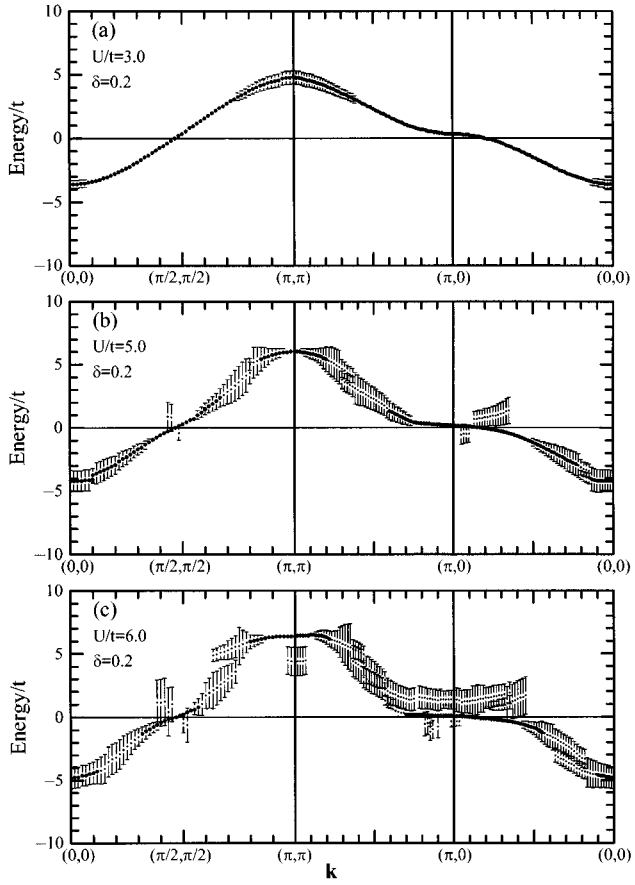

FIG. 9. Band dispersions for $\delta=0.2$, for (a) $U/t=3.0$, (b) 5.0, and (c) 6.0. The dispersion dots were extracted from data of the spectral functions. The error bar on each dot represents a broadening of the spectral function around the point. The solid circles represent points corresponding to relatively large intensity.

of the breakdown of the Fermi-liquid theory. However, we should note that the parameters used by them are $U/t=2.0$, at most, and the chemical potential $\mu=-0.375$, which corresponds to a doping $\delta\sim0.18$ for the noninteracting ($U/t=0.0$) system. These parameters are too weak to show the formation of the pseudogap in our scheme.

In Fig. 8 we plot the spectral function $A(\mathbf{k},\omega)$ for the (1,1) direction in the Brillouin zone for several values of the interaction U. Besides, in Fig. 9, we also plot the peak posi-

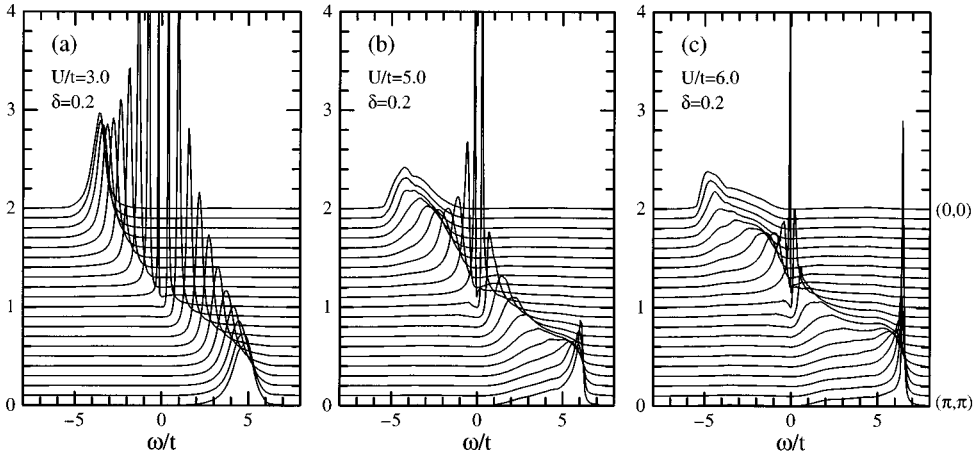

FIG. 8. Spectral functions $A(\mathbf{k},\omega)$ for the (1,1) direction calculated at $\delta=0.2$, for (a) $U/t=3.0$, (b) 5.0, and (c) 6.0. Each spectral function is shifted and the top (bottom) corresponds to $\mathbf{k}=(0,0)$ $(\mathbf{k}=(\pi,\pi))$.

tions that are extracted from the results obtained for the spectral functions. The sequence of the peak points may roughly correspond to band dispersions. The vertical line on each point indicates the relative intensity of the spectral function at the peak point. For $U/t=3.0$, in the low-energy region around the Fermi energy, the spectral function has a finite width but is sharply peaked. In contrast, in the high-energy region, the spectral function becomes broad. This produces the already mentioned band tails of the density of states in the high-energy region. The band dispersion is almost similar to that of the noninteracting tight-binding band for this parameter. For $U/t=5.0$, the broadening of the band edges becomes larger and the band dispersion has some discontinuous points. For $U/t=6.0$, only near the Fermi energy, we observe a sharp spectral weight and, in the high-energy region a new peak structure appears. The splitting in the dispersion becomes clear. The dispersion splits into three branches. Two of them, located in high-energy regions, correspond to the lower and the upper Hubbard band. The other, crossing the Fermi energy, is the quasiparticle band and its dispersion around the Fermi energy is much narrower than that for $U/t=3.0$. We emphasize that for large U/t, the quasiparticle band is no longer specified by a single continuous dispersion with a sharp clear peak, unlike the noninteracting band. The spectrum of the quasiparticle band has a clear sharp structure only near the Fermi surface.

These features are a natural consequence of the effects observed in the real and the imaginary parts of the self-energy. To see this we shall return to the plot of $\mathrm{Re}\Sigma(\mathbf{k},\omega)-\mu_*$ shown in Fig. 6. The dashed line in the figure represents $\omega-\varepsilon_{\mathbf{k}}$ at each $\mathbf{k}$. The ω coordinate of the intersection point of $\mathrm{Re}\Sigma(\mathbf{k},\omega)-\mu_*$ and the line of $\omega-\varepsilon_{\mathbf{k}}$ gives the ω pole of the Green's function. In the same way, the intersection of $\omega-\varepsilon_{\mathbf{k}}$ and the ω axis determines the pole of the mean-field Green's function. The shift of the poles (ω coordinate) represents roughly the shift of energy band from its mean-field value. Note that in the high-energy region the shift of poles for $U/t=6.0$ is considerably larger than that obtained for $U/t=3.0$. This shift gives the origin of the upper and the lower Hubbard bands. Note that as we follow the poles from the $\omega<0$ to the $\omega>0$ regions, if the direction of the shift of poles changes from negative to positive, the split of the band dispersion should take place at this point.

Moreover, we calculated the electronic states at the doping $\delta=0.5$. Since the increase in doping loosens the Stoner criterion, we can calculate for larger values of U/t. In Fig. 10 we show the DOS for $U/t=0.0$ (dotted line), 6.0 (dashed line), 8.0 (dashed-dotted line), and 10.0 (solid line). As U/t becomes larger, the large pseudogap arises around $\omega=4.0$. For $U/t=10.0$, a clear mini pseudogap appears at $\omega=-0.4$. The van Hove singularity moves toward the Fermi energy due to the band narrowing effect and the intensity of the peak becomes weaker due to the contribution of the imaginary part of the self-energy. In Fig. 11 we plot the band dispersion for the same doping and for $U/t=10.0$. There are clearly three dispersions that correspond to the upper and the lower Hubbard bands and to the quasiparticle band crossing the Fermi energy.

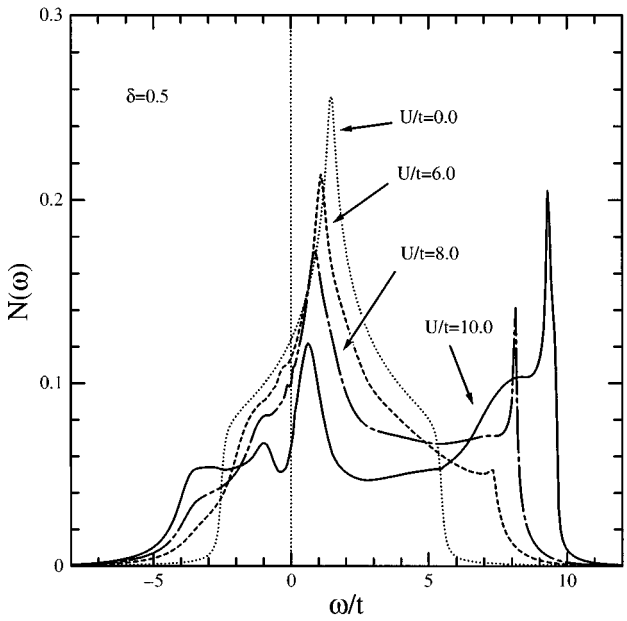

FIG. 10. Density of states at $\delta=0.5$, for $U/t=0.0$ (dotted line), 6.0 (dashed line), 8.0 (dashed-dotted line), and 10.0 (solid line).

VI. DISCUSSION

The density of states of the two-dimensional Hubbard model was calculated by Kampf and Schrieffer in a RPA treatment.[28] They took into account the spin fluctuation effect in the fermion self-energy and their treatment is related to our approximation. The differences in both formulations are the coupling constants on the vertex of the self-energy and the fact that we considered the charge fluctuation and they did not. It is interesting to compare their density of states with ours. The overall structures of the two density of states are similar but the quasiparticle peak on the Fermi energy is not observed in their data. In our results it can be seen that the quasiparticle band comes out into the pseudogap, which also appears in their results. Another important difference concerns the Stoner criterion. In our approach this criterion is weaker than it would be in the usual RPA-type theory and because of this we can perform calculations for larger values of U. This is an advantage of our method. Maybe one of the reasons why the quasiparticle band does not appear in the previous spin-fluctuation calculation[28] is that this approach is too sensitive with respect to the change in U, moreover, as we have shown in Fig. 3, the charge components of the self-energy keeps its Fermi-liquid-like energy dependence.

In our numerical analysis we have used the maximum values of the interaction $U/t=6.0$ and 10.0 for the fixed doping concentrations $\delta=0.2$ and 0.5, respectively. Because of the Stoner criterion we can not take a larger U/t, at least within the present approximate treatment of the Green's function and their self-energies. In this sense, our treatment is valid from the weak-coupling regime to the intermediate-coupling regime. To improve our approximation we should consider higher-order diagrams together with vertex corrections in the self-energies. In such a treatment the Coulomb interaction must be well renormalized and it will be replaced by the effective interaction. As a result, the Stoner criterion is weaker, and it will then be possible to investigate elec-

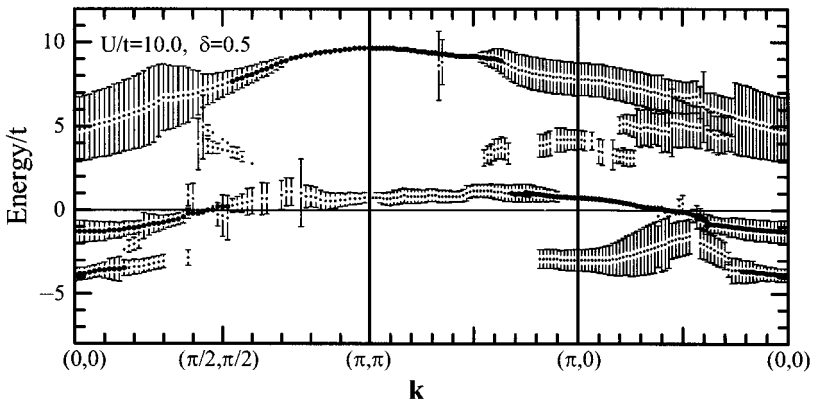

FIG. 11. Band dispersions at $\delta=0.5$ and for $U/t=10.0$. The dispersion dots were extracted from data of the spectral functions. The error bar on each dot represents a broadening of the spectral function around the point. The solid circles represent points corresponding to relatively large intensity.

tronic states at the very low dopings and larger U's, i.e., close to the metal-insulator transition. Another important improvement is to solve the coupled Dyson equations of the fermion and the boson propagators self-consistently. We plan to investigate these directions in the future.

The energy dependence of the real part of the self-energy is important in characterizing the properties of the Fermi liquid. The energy derivative of the real part of the self-energy at the Fermi energy $\omega=0$ relates to the residue $z_{\mathbf{k}_F}$ of the quasiparticle Green's function by

$$z_{\mathbf{k}_F}=\left(1-\frac{\partial \mathrm{Re}\Sigma(\mathbf{k}_F,\omega)}{\partial\omega}\bigg|_{\omega=0}\right)^{-1}$$
$$=\left[1-\left(3\frac{\partial \mathrm{Re}\Sigma_s(\mathbf{k}_F,\omega)}{\partial\omega}\bigg|_{\omega=0}+\frac{\partial \mathrm{Re}\Sigma_c(\mathbf{k}_F,\omega)}{\partial\omega}\bigg|_{\omega=0}\right)\right]^{-1}. \tag{6.1}$$

The band narrowing effect of the quasiparticle band is produced by $z_{\mathbf{k}_F}$. If we neglect the fact that $\mathrm{Im}\Sigma_s(\mathbf{k},\omega)$ scales linearly with ω when $\omega\to 0$, we find the following relations. From Fig. 3, we can see that the slope of the spin component is larger than that of the charge component and the difference becomes larger as U/t becomes large. The quasiparticle band narrowing effect comes from the spin component of the real part of the fermion self-energy. To see this more clearly we separate $z_{\mathbf{k}_F}$ into their spin and charge parts. By defining the z factors associated with the charge and spin fluctuations as

$$z^{-1}_{\alpha\mathbf{k}_F}=1-4\frac{\partial \mathrm{Re}\Sigma_\alpha(\mathbf{k}_F,\omega)}{\partial\omega}\bigg|_{\omega=0}, \tag{6.2}$$

where $\alpha=c$, s, we find that $z_{\mathbf{k}_F}$ is given by

$$z^{-1}_{\mathbf{k}_F}=\frac{z^{-1}_{c\mathbf{k}_F}+3z^{-1}_{s\mathbf{k}_F}}{4}, \tag{6.3}$$

or, equivalently,

$$z_{\mathbf{k}_F}=\frac{4z_{c\mathbf{k}_F}z_{s\mathbf{k}_F}}{z_{s\mathbf{k}_F}+3z_{c\mathbf{k}_F}}. \tag{6.4}$$

Further by introducing the effective mass m^* in the form of $m^*\sim z^{-1}m_0$ with m_0 being the noninteracting electron mass,[29] from Eq. (6.3), it follows that the quasiparticle effective mass and its components coupled with the charge fluctuation (m_c^*) and spin fluctuation (m_s^*) are related by

$$m^*\sim\frac{m_c^*+3m_s^*}{4}, \tag{6.5}$$

with $m^*\sim z^{-1}_{\mathbf{k}_F}m_0$, $m_c^*\sim z^{-1}_{c\mathbf{k}_F}m_0$, and $m_s^*\sim z^{-1}_{s\mathbf{k}_F}m_0$. Thus, the above-mentioned behavior of the slope in the real part of the self-energy, around the Fermi energy, produces the enhancement of the quasiparticle mass coupled with the spin fluctuation, which is much larger than that of the charge-fluctuation counterparts, i.e., $m_s^*>m_c^*$.

Recent angle-resolved photoemission spectrum experiments[4,5,30] for high-T_c materials provide important features of the low-energy spectral function in these materials. One of the remarkable features is the existence of the strikingly ''flat'' dispersion of the band around $\mathbf{k}=(\pi,0)$. This tendency of the quasiparticle band is observed in our results as seen in Fig. 9(c). In the present approach this is understood as the band narrowing effect naturally arising by the self-energy effects. We should note that since the single-band Hubbard model is rather simple, if we use the model to explain experimental facts of the high-T_c materials, we have to pay attention to the limits of its applicability. For a more detailed comparison with experimental data, it might be necessary to exploit a more realistic model such as the Hubbard model including the next-nearest-neighbor hopping term[18] or the CuO_2 (d-p) model.

Let us compare our results with the data obtained in some numerical simulations of the finite-size cluster Hubbard model. In the density of states studied in the quantum Monte Carlo (QMC) simulations by Bulut, Scalapino, and White,[16] a narrow coherent band is observed on the Fermi energy for small doping $\delta=0.13$ for $U/t=4.0$ and also $U/t=8.0$. The corresponding quasiparticle band in our data is narrower than theirs. Since their results are at finite temperature, the bandwidth must be broader than at $T=0$. For small doping $\delta=0.13$ and for $U/t=8.0$, their data show the existence of lower and upper Hubbard bands and also a pseudogap in the high-energy region. Similar structure has been obtained also in our results for moderate doping $\delta=0.5$ and $U/t=10.0$. However, a large pseudogap has not been observed in our

results for $\delta=0.2$ and $U/t=6.0$. Rather, our results for the parameters are similar to their results for $\delta=0.13$ and $U/t=4.0$. The origin will be our approximate treatment and the relatively small value of U/t.

In the exact-diagonalization calculation,[13–15] a prominent sharp band peak in the spectral function has been observed at the wave number $\mathbf{k}$ around the Fermi surface. The intensity of the peak becomes weaker as $\mathbf{k}$ goes further away from the Fermi momentum. Here again, in the high-energy region, there exists a broad band corresponding to the lower and upper Hubbard bands. These features were observed also in our results for the spectral functions. In our results of the density of states, a strong peak appears at the high-energy edge of the band. Such a strange peak is not seen in the numerical simulations. It is just the result of the weak tail of the imaginary part of the self-energy and is a result of our approximate method.

Very recently, Preuss *et al.*[19] calculated a band dispersion of the Hubbard model for dopings very close to half filling by a QMC simulation with maximum-entropy method. Their data have shown that a ''flat'' band crosses the Fermi level at $\mathbf{k}=(\pi,0)$ point when the doping concentration approaches half filling. If the Luttinger theorem of the Fermi surface volume holds in this case, the result means that the electronlike Fermi surface transforms into the holelike one by doping reduction. In our results of the band dispersions shown in Fig. 9 band crossing is not seen. However, the ''flat'' band near $\mathbf{k}=(\pi,0)$ approaches the Fermi energy as the interaction becomes large. Furthermore, from Fig. 11, we find that the bandwidth of the quasiparticle band can be estimated as being approximately $5J/t$ with $J=4t^2/U$. This is similar to their results $\sim 4J/t$ calculated for $U/t=8.0$ and at $\delta=0.05$. Although this similarity seems strange because our doping is $\delta=0.5$, this originates from the fact that in our calculation the parameter is close to the Stoner condition. The overall structure of our band dispersion is very similar to their results. In conclusion our results reproduce qualitatively the results obtained in the numerical simulations.

VII. SUMMARY AND CONCLUSIONS

In this paper we studied the behavior of the electronic states of the two-dimensional Hubbard model in the doped paramagnetic regime. We considered both the charge and the spin fluctuations on an equal footing. Auxiliary bosons were introduced in our treatment for fluctuations. The fermion-boson interactions were taken into account up to the one-loop level in the self-energies. The single-particle Green's function, which goes beyond the mean-field level, includes the self-energy effects thorough the corresponding Dyson equation. By representing the interaction Hamiltonian using both the charge- and the spin-density operators, the Stoner condition became weaker than the one based on the usual U perturbation treatment. It allowed us to evaluate the single-particle Green's function for the moderately large interaction U. The evolution of the single particle spectrum was investigated by numerical calculations of the boson propagators and the Green's function with the self-energy as we vary U/t.

As U approaches the critical value for the magnetic instability, the low-energy spin excitation is strongly enhanced at the paramagnon peak, which has the wave vector $\mathbf{q}$ near $2\mathbf{k}_F$. The sharp enhancement of the spin excitation modifies the energy dependence of both the imaginary part and the real part of the fermion self-energy around the Fermi energy. In particular, near the Fermi surface, the imaginary part of the self-energy shows the characteristic ω linear dependence of a non-Fermi liquid. The calculated spectral function shows the existence of the band splitting and the band narrowing on the Fermi energy. As a result of this, we have found the pseudogap in the density of states. This seems to be an important feature to understand the spin-gap phenomena in the experimentally observed spin excitation spectrum. These striking changes in the band structure are produced by the change of the energy dependence of the self-energy due to enhancement of the spin fluctuations close to the Stoner criterion. Our results on the single-particle spectra are in qualitative agreement with the data of the numerical calculations of the finite-size clusters.

ACKNOWLEDGMENTS

We would like to acknowledge useful discussions with Dr. S. L. Garavelli, Dr. X. Xue, and other members of the International Center of Condensed Matter Physics. We would like to thank C. Ohmori for his useful advice on the computer program. We also would like to thank Professor H. Matsumoto for his useful suggestion. This work was supported by the Conselho Nacional de Desenvolvimento Científico e Tecnológico (CNPq) and by the Financiadora de Estudos e Projetos (FINEP). One of us (T.S.) would like to acknowledge support by the Kasuya Research Fund, Japan, before coming to Brazil. The numerical calculations were performed by use of the supercomputing system at the Institute for Materials Research, Tohoku University, Japan.

APPENDIX CALCULATION OF $\mathrm{Im}\chi_0(\mathbf{q}\nu)$

In this Appendix we illustrate briefly how to calculate the imaginary part of the one-loop polarization function given by Eq. (4.4). We change the $\mathbf{k}$ summation into the integral in the first Brillouin zone. Then we have

$$\mathrm{Im}\chi_0(\mathbf{q},\nu)=\pi\mathrm{sgn}(\nu)\int\frac{d\mathbf{k}}{(2\pi)^2}[\theta(\varepsilon_{\mathbf{k}+\mathbf{q}}-\mu_0)-\theta(\varepsilon_{\mathbf{k}}-\mu_0)]\delta(\nu-\varepsilon_{\mathbf{k}+\mathbf{q}}+\varepsilon_{\mathbf{k}}). \quad \text{(A1)}$$

Since this $\mathbf{k}$ integral includes the δ function that depends on the two-dimensional wave vector $\mathbf{k}$, it is rather difficult to perform this integration numerically to a good accuracy. We consider the way to avoid this difficulty.

When we fix both $\mathbf{q}$ and ν, the contribution to the integral comes from a sequence of points on a curve in the first Brillouin zone. The curve is obtained by the energy conservation relation given by

$$\nu=\varepsilon_{\mathbf{k}+\mathbf{q}}-\varepsilon_{\mathbf{k}} \quad \text{(A2)}$$

in the δ function. It tells us that we can rewrite the two-dimensional integral as a contour integral on the line. Performing the integral of one variable that is perpendicular to the contour, we have the contour integral as

$$\mathrm{Im}\chi_0(\mathbf{q},\nu)=\pi\mathrm{sgn}(\nu)\int_{\nu=\varepsilon_{\mathbf{k}+\mathbf{q}}-\varepsilon_{\mathbf{k}}}\frac{dl_{\mathbf{k}}}{(2\pi)^2}\frac{\theta(\varepsilon_{\mathbf{k}+\mathbf{q}}-\mu_0)-\theta(\varepsilon_{\mathbf{k}}-\mu_0)}{|\mathrm{grad}_{\mathbf{k}}(\varepsilon_{\mathbf{k}+\mathbf{q}}-\varepsilon_{\mathbf{k}})|}. \tag{A3}$$

The contour of the integral is obtained by solving Eq. (A2). We find solution of this as

$$\cos k_y=\frac{-(1-\cos q_y)f_1\pm\sqrt{(1-\cos q_y)^2f_1-2(1-\cos q_y)(f_1^2-\sin^2 q_y)}}{2(1-\cos q_y)}, \tag{A4}$$

where f_1 is given by

$$f_1(k_x,q_x,\nu)=-\frac{\nu}{2t}+\cos k_x(1-\cos q_x)+\sin k_x\sin q_x. \tag{A5}$$

When we both fix $\mathbf{q}$ and ν, we obtain a contour equation from this solution. Thus, we can perform the integral without dealing with the difficulty of the numerical treatment of the δ function. Strictly speaking, the exact contribution range in the $\mathbf{k}$ space is determined by the superposition of the above solution and the region that satisfies the condition $\theta(\varepsilon_{\mathbf{k}+\mathbf{q}}-\mu_0)-\theta(\varepsilon_{\mathbf{k}}-\mu_0)\neq 0$.

We can apply this method to the other model. For example, Saikawa and Kaga have calculated fermion bubbles of the three-band CuO_2 model using this method.[31] However, if we consider a complicated model such as the CuO_2 model, we can not obtain the analytical form of the contour of the integration because such a model often has a complicated (mean-field) band dispersion. In such a case we need to obtain the contour numerically.

*Present address: Department of Physics, Tokyo Institute of Technology, Tokyo 152, Japan.

[1] For example, Physica C **263** (1996).
[2] H. Yasuoka, T. Imai, and T. Shimizu, in *Strong Correlation and Superconductivity*, edited by H. Fukuyama, S. Maekawa, and A. P. Malaozemoff (Springer-Verlag, Berlin, 1989).
[3] J. Rossat-Mignod *et al.*, Physica C **185-189**, 86 (1991).
[4] J. W. Loram *et al.*, Physica C **235-240**, 134 (1994).
[5] A. G. Loeser *et al.*, Science **273**, 325 (1996); A. G. Loeser, D. S. Dessau, and Z.-X. Shen, Physica C **263**, 208 (1996).
[6] Y. Suzumura, Y. Hasegawa, and H. Fukuyama, J. Phys. Soc. Jpn. **57**, 2768 (1988).
[7] H. Fukuyama, Physica C **263**, 35 (1996).
[8] Y. C. Chen *et al.*, Phys. Rev. B **50**, 655 (1994).
[9] J. Hubbard, Proc. R. Soc. London, Ser. A **276**, 238 (1963); **277**, 237 (1964); **281**, 401 (1964).
[10] W. F. Brinkman and T. M. Rice, Phys. Rev. B **2**, 4302 (1970).
[11] R. Raimondi and C. Castellani, Phys. Rev. B **48**, 11 453 (1993).
[12] E. Dagotto, Rev. Mod. Phys. **66**, 763 (1994).
[13] E. Dagotto, *et al.*, Phys. Rev. B **45**, 10 741 (1992).
[14] P. W. Leung *et al.*, Phys. Rev. B **46**, 11 779 (1992).
[15] H. Eskes and R. Eder, Phys. Rev. B **54**, R14 226 (1996).
[16] N. Bulut, D. J. Scalapino, and S. R. White, Phys. Rev. Lett. **72**, 705 (1994).
[17] N. Bulut, D. J. Scalapino, and S. R. White, Phys. Rev. Lett. **73**, 748 (1994).
[18] D. Duffy *et al.* (unpublished).
[19] R. Preuss, W. Hanke, C. Gröber, and H. G. Evertz (unpublished).
[20] A. Georges, G. Kotliar, W. Krauth, and M. J. Rozemberg, Rev. Mod. Phys. **68**, 13 (1996), and references therein.
[21] H. Matsumoto and F. Mancini, Phys. Rev. B **55**, 2095 (1997).
[22] See for example, S. Doniach and E. H. Sondheimer, *Green's Functions for Solid State Physicists* (Addison-Wesley, New York, 1974).
[23] See, for example, E. Fradkin, *Field Theories of Condensed Matter Systems* (Addison-Wesley, New York, 1991). In some parts of our text we have followed the notations of this book.
[24] A. Ferraz and Nguyen Ai Viet, Phys. Rev. B **51**, 10 548 (1995); X. Xue and A. Ferraz, Nucl. Phys. B **468**, [FS]541 (1996).
[25] P. E. de Brito, Ph.D. thesis, Universidade de Brasília, 1996.
[26] S. Doniach, Proc. Phys. Soc. London **91**, 86 (1967). See also, Ref. 22.
[27] See for example, G. D. Mahan, *Many-Particle Physics*, 2nd ed. (Plenum, New York, 1990).
[28] A. Kampf and J. R. Schrieffer, Phys. Rev. B **41**, 6399 (1990).
[29] The effective mass on the Fermi surface should be defined by $m/m^*=(\partial E_{\mathbf{k}}/\partial\varepsilon_{\mathbf{k}})_{\mathbf{k}=\mathbf{k}_F}$ where $E_{\mathbf{k}}$ is a quasiparticle band defined as the solution of the equation given by $E_{\mathbf{k}}+\mu-\varepsilon_{\mathbf{k}}-\mathrm{Re}\Sigma(\mathbf{k},E_{\mathbf{k}})=0$. From this definition, the effective mass is given by $m/m^*=z_{\mathbf{k}_F}\{1+[\partial\mathrm{Re}\Sigma(\mathbf{k},\omega)/\partial\varepsilon_{\mathbf{k}}]_{\mathbf{k}=\mathbf{k}_F,\omega=0}\}$. [See, for example, *Many-Particle Physics* (Ref. 27), Chap. 3.] In our discussion the $\mathbf{k}$ derivative of $\mathrm{Re}\Sigma(\mathbf{k},\omega)$ is omitted.
[30] Z.-X. Shen and D. S. Dessau, Phys. Rep. **253**, 1 (1995), see also references therein.
[31] T. Saikawa and H. Kaga, Physica C **217**, 210 (1993); **221**, 413 (1994).